International Journal of Chronic Obstructive Pulmonary Disease Dovepress
open access to scientific and medical research

Open Access Full Text Article ORIGINAL RESEARCH

Lianhua Qingke Preserves Mucociliary Clearance in Rat with Acute Exacerbation of Chronic Obstructive Pulmonary Disease by Maintaining Ciliated Cells Proportion and Protecting Structural Integrity and Beat Function of Cilia

Xiaoqi Wang[1,2], Yuanjie Hao[3], Yujie Yin[4,5], Yunlong Hou[2,4,5], Ningxin Han[3], Yi Liu[3], Zhen Li[3], Yaru Wei[1], Kun Ma[1], Jiaojiao Gu[1], Yan Ma[1], Hui Qi[4,5], Zhenhua Jia[1,4–6]

[1]Graduate School, Hebei University of Chinese Medicine, Shijiazhuang, Hebei, 050090, People's Republic of China; [2]Hebei Yiling Pharmaceutical Research Institute, Shijiazhuang, 050035, People's Republic of China; [3]Graduate School, Hebei Medical University, Shijiazhuang, Hebei, 050017, People's Republic of China; [4]Hebei Academy of Integrated Traditional Chinese and Western Medicine, Shijiazhuang, Hebei, 050035, People's Republic of China; [5]National Key Laboratory for Innovation and Transformation of Luobing Theory, Shijiazhuang, 050035, People's Republic of China; [6]Department of Respiratory, Affiliated Yiling Hospital of Hebei Medical University, Shijiazhuang, Hebei, 050091, People's Republic of China

Correspondence: Zhenhua Jia, Graduate School, Hebei University of Chinese Medicine, Shijiazhuang, Hebei, 050090, People's Republic of China, Email jzhjiazhenhua@163.com; Hui Qi, Hebei Academy of Integrated Traditional Chinese and Western Medicine, Shijiazhuang, Hebei, 050035, People's Republic of China, Email qihui_qh@163.com

International Journal of Chronic Obstructive Pulmonary Disease downloaded from https://www.dovepress.com/
For personal use only.

Purpose: Acute Exacerbation of Chronic Obstructive Pulmonary Disease (AECOPD) is a sudden worsening of symptoms in patients with Chronic Obstructive Pulmonary Disease (COPD), such as cough, increased sputum volume, and sputum purulence. COPD and AECOPD are characterized by damage to cilia and increased mucus secretion. Mucociliary clearance (MCC) functions as part of the primary innate system of the lung to remove harmful particles and pathogens together with airway mucus and is therefore crucial for patients with COPD.

Methods: AECOPD was induced by cigarette smoke exposure (80 cigarettes/day, 5 days/week for 12 weeks) and lipopolysaccharide (LPS) instillation (200 μg, on days 1, 14, and 84). Rats administered Lianhua Qingke (LHQK) (0.367, 0.732, and 1.465 g/kg/d) or Eucalyptol, Limonene, and Pinene Enteric Soft Capsules (ELP, 0.3 g/kg/d) intragastrically. Pulmonary pathology, Muc5ac+ goblet cell and β-tubulin IV+ ciliated cells, and mRNA levels of forkhead box J1 (Foxj1) and multiciliate differentiation and DNA synthesis associated cell cycle protein (MCIDAS) were assessed by hematoxylin and eosin staining, immunofluorescence staining, and RT-qPCR, respectively. Ciliary morphology and ultrastructure were examined through scanning electron microscopy and transmission electron microscopy. Ciliary beat frequency (CBF) was recorded using a high-speed camera.

Results: Compared to the model group, LHQK treatment groups showed a reduction in inflammatory cell infiltration, significantly reduced goblet cell and increased ciliated cell proportion. LHQK significantly upregulated mRNA levels of MCIDAS and Foxj1, indicating promoted ciliated cell differentiation. LHQK protected ciliary structure and maintained ciliary function via increasing the ciliary length and density, reducing ciliary ultrastructure damage, and ameliorating random ciliary oscillations, consequently enhancing CBF.

Conclusion: LHQK enhances the MCC capability of ciliated cells in rat with AECOPD by preserving the structural integrity and beating function of cilia, indicating its therapeutic potential on promoting sputum expulsion in patients with AECOPD.

Keywords: goblet hyperplasia, ciliary density, ciliary length, ciliary ultrastructure, ciliary beat frequency, CBF

Introduction

Chronic Obstructive Pulmonary Disease (COPD) is a respiratory disorder distinguished by a gradual and irreversible constriction of airflow, accompanied by persistent inflammation resulting from exposure to detrimental environmental

Received: 22 September 2023
Accepted: 26 December 2023
Published: 7 February 2024

© 2024 Wang et al. This work is published and licensed by Dove Medical Press Limited. The full terms of this license are available at https://www.dovepress.com/terms.php and incorporate the Creative Commons Attribution – Non Commercial (unported, v3.0) License (http://creativecommons.org/licenses/by-nc/3.0/). By accessing the work you hereby accept the Terms. Non-commercial uses of the work are permitted without any further permission from Dove Medical Press Limited, provided the work is properly attributed. For permission for commercial use of this work, please see paragraphs 4.2 and 5 of our Terms (https://www.dovepress.com/terms.php).

agents such as tobacco smoke and fumes.[1,2] Acute exacerbation of chronic obstructive pulmonary disease (AECOPD) refers to a sudden occurrence marked by the deterioration of respiratory symptoms, including increased coughing, sputum volume, and purulence.[3] This deterioration of health status can lead to a decline in lung function, an increase in hospitalization, an accelerated progression of the disease, and a significant social and economic burden for patients with COPD.[4]

In patients with AECOPD, excessive secretion of mucus (due to bacterial or viral infections) can obstruct airways, and impair the clearance of pathogens and other inhaled microorganisms, leading to a vicious cycle of infection and injury[5,6] and 3.5 times higher death risk.[7,8] Mucociliary clearance (MCC) is the primary defense mechanism that removes harmful particles and pathogens, along with mucus, from the airways to protect the pulmonary system.[9] Ciliated cells, a main cell type of airway epithelium, provide the force necessary for MCC. Cilia on the surface of ciliated cells are the main component of the MCC system and regularly and continuously beat in the mucous layer to expel harmful particles and pathogens out of the airways.[10–12] Structure–function studies have proven that ciliary characteristics including structure, number, ciliary beat frequency (CBF), ciliary wave pattern, and ciliary orientation are important for proper ciliary function and can be altered in AECOPD,[13,14] leading to the accumulation of mucus.[15] Given that the ciliary system plays a crucial role in resolving mucus hypersecretion,[16–19] pharmaceutical interventions aimed at modulating the proportion of ciliated cells, and the structural and beat function of cilia, exhibit potential in mitigating airway mucus hypersecretion and providing therapeutic benefits to patients affected by respiratory obstruction.

Under the guidance of the theory of collateral disease, Lianhua Qingke (LHQK), a novel traditional Chinese medicine (TCM), was developed from two TCM preparations: Maxing Shigan decoction and Qingjin Huatan decoction.[20–22] LHQK is clinically used for acute tracheobronchitis, cough, and other respiratory diseases. Experimental and clinical evidence has demonstrated the therapeutic effects of LHQK in reducing sputum production[23] and viscosity.[24] In addition, LHQK has been proven to be effective in promoting sputum expulsion in both animal models and patients.[25] This study investigated the therapeutic effects and underlying mechanisms of LHQK in a rat model of AECOPD induced by cigarette smoke (CS) exposure and lipopolysaccharide (LPS) intratracheal instillation. The results demonstrated that LHQK can effectively preserve MCC in AECOPD by maintaining the proportion of ciliated cells, as well as the ciliary structure and beating function of cilia.

Materials and Methods

Animals

All animal experiments conducted in this study were carried out in strict accordance with the guidelines of the Guiding Principles in the Care and Use of Animals (China) and were approved by Experimental Animal Ethical Committee of Hebei Yiling Pharmaceutical Research Institute (No. N2021162). Six-week-old male Wistar rats (180–220 g) were bought from Beijing Weitong Lihua Experimental Animal Technology Co., Ltd. (Beijing, China). The rats were randomly divided into six groups (n = 10): control group (room air exposure), model group (CS+LPS), LHQK low-dose group (LHQK-L), LHQK middle-dose group (LHQK-M), LHQK high dose group (LHQK-H), and eucalyptus lime-pinenteric soft capsule (ELP) group. Except rats in the control group, rats in all other groups were subjected to CS+LPS exposure to induce the AECOPD model. Rats in the control and CS+LPS groups received intragastric administration of a 0.5% carboxymethylcellulose (CMC) sodium solution, whereas rats in the LHQK-L, LHQK-M, and LHQK-H groups were subjected to intragastric administration of LHQK at doses of 0.367, 0.732, and 1.465 g/kg/d, respectively, which correspond to 0.5, 1, and 2 times of the clinical doses used for human patients. Eucalyptol, Limonene, and Pinene Enteric Soft Capsule (ELP), a mucus soluble expectorant, was used as the positive control for this study. ELP (0.3 g/kg/d) was administered by gavage to the rats in the ELP group. LHQK and ELP were administered daily over a period of 12 weeks, starting from the first day of cigarette smoke (CS) exposure. The AECOPD model was established by 12 weeks of CS exposure (80 cigarettes/day for 5 days per week, 2 hr per day) and intratracheal instillation of LPS (055: B5, L2880, Sigma, USA) instillation. The commercial cigarettes were produced by Shanghai Tobacco Industry Co., Ltd. (Hongshuangxi Filter Cigarette, Shanghai, China). A dose of 200 μg of LPS (prepared as 1 mg/mL solution in saline) was instilled intratracheally on days 1, 14, and 84 after the rats were anesthetized with 5% isoflurane. Before collecting

samples on day 85, which occurred 24 hr after the final LPS instillation, the rats were anesthetized by intraperitoneal injection of 2% pentobarbital sodium at a dosage of 3 mL/kg.

Sample Solution Preparation

LHQK tablets (Lot No. 2104001) were provided by Shijiazhuang Yiling Pharmaceutical Co., Ltd. (Shijiazhuang, China). The recipe of LHQK is composed of *Ephedra sinica* Stapf (Ephedraceae), *Forsythia suspensa* (Thunb.) Vahl (Oleoideae), *Scutellaria baicalensis* Georgi (Labiatae), *Morus alba* L. (Moraceae), *Prunus sibirica* L. (Rosaceae), *Peucedanum praeruptorum* Dunn (Umbelliferae), *Pinellia ternate* (Thunb.) Breit. (Araceae), *Citrus reticulata* Blanco (Rutaceae), *Fritillaria thunbergii* Miq. (Liliaceae), *Arctium lappa* L. (Compositae), *Lonicera japonica* Thunb. (Caprifoliaceae), *Rheum palmatum* L. (Polygonaceae), *Platycodon grandiflorus* (Jacq.) A. DC. (Campanulaceae), *Glycyrrhiza uralensis* Fisch. (Leguminosae), and Gypsum fibrosum. The LHQK tablets were dissolved in 0.5% CMC sodium solution to obtain solutions of concentrations 0.0367, 0.0732, and 0.1465 g/mL.

ELP was obtained from Beijing Jiuhe Pharmaceutical Co., Ltd (Beijing, China) and dissolved in 0.5% CMC sodium solution to obtain a solution of concentration with 0.3 g/mL.

Hematoxylin and Eosin (HE) Staining

After anesthesia, 3 mL of 4% paraformaldehyde solution was perfused into the left lobe of the lung via the trachea. Following perfusion, lung tissues were dissected and promptly immersed in a 4% paraformaldehyde solution for fixation. Subsequently, they underwent dehydration using a series of alcohol solutions with varying concentrations, followed by embedding in paraffin. The embedded tissues were then sectioned, deparaffinized, and subjected to staining with hematoxylin and eosin (H&E) using a commercial kit (Beyotime, Shanghai, China). Finally, the resulting slices were captured using a fully automated biological microscope (Leica DM6000B, Wetzlar, Germany).

Immunofluorescence (IF) Staining

Rat tracheas were fixed using a 4% paraformaldehyde solution, subsequently dehydrated following standard protocols, embedded in paraffin, and sliced into sections measuring 5 μm. The sectioned tracheas underwent deparaffinization and were subsequently subjected to antigen retrieval in 1 mM Tris/EDTA buffer (pH 9.0) before washed with phosphate-buffered saline (PBS). The sections were then incubated with hydrogen peroxide for 10 min at 37°C in the dark. Following this, the sections were blocked using a 5% solution of bovine serum albumin (BSA) for a duration of 30 min at room temperature. Subsequently, the sections were subjected to incubation with primary antibodies targeting β-tubulin IV (Abcam, 1:500, Cambridge, UK) at a temperature of 4°C overnight. The sections were subsequently rinsed with PBS and exposed to a fluorescent conjugate secondary antibody (Goat anti-rabbit IgG H&L, Alexa Fluor® 594, Abcam, 1:500) for a duration of 50 min at room temperature in the dark. Following this, the sections were stained with 4′,6-diamidino-2-phenylindole (DAPI) (Solarbio, Beijing, China). Ultimately, the sections were examined using a Zeiss confocal microscope (Oberkochen, Germany). Information for all antibodies used in this study are listed in Table 1.

Immunohistochemistry (IHC)

Tissue paraffin samples were sectioned into 5-μm slices, which were subsequently subjected to a heat treatment in 1 mM ethylenediaminetetraacetic acid (EDTA) at 95°C for 20 min. Following this, the sections were exposed to 3% hydrogen

Table 1 Antibodies Used in This Study

Antibodies	Company	Dilution
Anti-β-tubulin IV	Abcam, ab17959	1:500
Anti-Muc5ac	Abcam, ab3649	1:2000
Anti-GAPDH	Abcam, ab181602	1:1000
Goat Anti-Rabbit IgG H&L	Abcam, ab150080	1:500
Goat anti-rabbit IgG H&L	Abcam, ab216777	1:10,000

peroxide for 20 min and then blocked with 10% goat serum for 90 min at room temperature. Subsequently, the sections were incubated overnight at 4°C with mice monoclonal anti-rat Muc5ac antibody (Abcam, ab3649, 1:2000, Cambridge, UK). The sections were washed in PBS and subjected to a 30 min incubation with a secondary antibody kit (Zhongshanjinqiao, Beijing, China) at a temperature of 37°C. Following another rinse in PBS, the sections were visualized using 3,3′-diaminobenzidine (DAB) as the developing agent. The resulting images were captured using a Leica light microscope.

The number of Muc5ac+ cells per μm of basal lamina was quantified. Briefly, three fields were randomly selected from each trachea ring section of five rats in each group, and the ImageJ software was employed to quantify the number of Muc5ac+ cells and the length of the basal lamina.

Western Blot Analysis

Proteins were extracted from rat tracheas using radioimmunoprecipitation assay (RIPA) lysis buffer containing the protease inhibitor phenylmethylsulfonyl fluoride (PMSF). Protein concentrations were evaluated using a bicinchoninic acid (BCA) protein assay kit (Biyuntian, China). An equal number of boiled protein samples were separated using 4–20% sodium dodecyl sulfate-polyacrylamide gel electrophoresis (SDS-PAGE) gels (GenScript Biotech Corporation, China). The separated proteins were then transferred onto polyvinylidene fluoride (PVDF) membranes (Life Sciences, Mexico). The membranes were subsequently blocked for 1 hr at 37°C using Odyssey® blocking buffer (LI-COR, Lincoln, Nebraska, USA). Following the blocking step, the membranes were incubated overnight at 4°C with rabbit monoclonal anti-rat antibody (β-tubulin IV, Abcam, 1:1000, Cambridge, UK). The membranes were subsequently subjected to three washes (each lasting 10 min) with tris-buffered saline containing Tween 20 (TBST) and subsequently exposed to fluorescent conjugate secondary antibodies (goat anti-rabbit IgG H&L) at a temperature of 37°C for 1 h. Following three additional washes with TBST, membranes were scanned using an Odyssey imager (LI-COR, Lincoln, Nebraska, USA). The internal reference utilized in this study was glyceraldehyde-3-phosphate dehydrogenase (GAPDH).

Real-Time Quantitative Polymerase Chain Reaction (RT-qPCR)

Total RNA was isolated from rat tracheal samples utilizing Trizol-Reagent (Invitrogen, Thermo, Waltham, MA). Reverse transcription was conducted utilizing the Prime Script™ RT Reagent Kit (Takara Bio, Kusatsu, Japan) to obtain cDNA, while RT-qPCR was executed employing the SYBR Green PCR Master Mix (Takara Bio, Kusatsu, Japan) in accordance with the manufacturer's guidelines. The PCRs were carried out and documented utilizing the QuantStudio RT-qPCR system (Thermo Fisher Scientific, Massachusetts, USA). The relative mRNA levels of target genes were calculated using the relative quantitative formula $2^{-\Delta\Delta Ct}$, where ΔCt value = target gene Ct value – GAPDH gene Ct value.[26] GAPDH was used as the internal control. The primer sequences are shown in Table 2.

Ex vivo CBF Analysis

CBF was analyzed based on the literature.[27] Briefly, rats were euthanized with pentobarbital (Merck, Darmstadt, Germany), and their tracheas were removed and placed in Dulbecco's modified eagle medium (DMEM). The main tracheas were cut into rings (0.5 mm in width) and maintained in DMEM for 20–30 min. The ciliary movement was

Table 2 Primer Sequences Used for RT-qPCR

Species	Genes	Primer Direction	Sequence (5′-3′)
Rat	Foxj1	Forward	CCAAGTACCGGGTTTGGTGG
		Reverse	TTCGAGATGTGCACGACGAT
	MCIDAS	Forward	GACAGCAAGGATTGCAGCAC
		Reverse	GAGTGCGGATGGTGCTATGG
	GAPDH	Forward	CTGGAGAAACCTGCCAAGTATG
		Reverse	GGTGGAAGAATGGGAGTTGCT

recorded in 3–5 different fields of view randomly selected under an inverted microscope (Olympus IX73, Tokyo, Japan) and phase contrast objective lens (40×) with a high-speed camera. The recordings were at a rate of 200–250 frames per second for 2.0–3.0 s. The images were imported into ImageJ to select 3–6 regions of interest (ROI), and the average gray value was measured within the ROI of each frame. A variation in the gray intensity of a single ROI is caused by the repetitive motion of the cilia. The beat period was calculated by dividing the number of full beats by the time consumed, with the mean ± standard deviation (SD) expressed in Hz.

In vitro CBF Analysis

Tracheas from the anesthetized rats were dissected and dissociated into single cells in a digestion buffer containing pronase E (100mg/mL; From *Streptomyces grays*, MCE, HY-114158A), DNase I (Solarbio, D8071, Beijing, China), and DMEM/F12 (Gibco, California, USA) for 18 h at 4°C. The dissociated cells were collected into a new tube with a culture medium containing 10% fetal bovine serum (FBS) and centrifuged at 4°C and 500 g for 10 min. The cell pellets were resuspended in 2 mL of an incubation medium and placed in 12-well plates. A total of 20 to 30 ciliated cells were randomly selected under a high-speed camera, inverted microscope, and phase contrast objective lens (40×). The ciliary movement was recorded and analyzed in a manner similar to that of tracheal ring CBF.

Scanning Electron Microscopy (SEM)

The tracheas obtained from the rats were fixed with a solution containing 2.5% glutaraldehyde and 1.5% paraformaldehyde in 0.1 M sodium phosphate buffer (pH 7.4) for 3 h at room temperature. Subsequently, the specimens were subjected to fixation for 2 hr in a solution consisting of 1% OsO4 in 0.1 M sodium phosphate buffer. Following dehydration in graded ethanol, the specimens underwent drying in a critical-point dryer (Quorum, K850, UK), were subsequently affixed onto stubs, and finally coated with gold-palladium in a cool sputter coater (HITACHI, MC1000, Tokyo, Japan). The samples were examined using a scanning electron microscope (SEM) (HITACHI, SU8100, Tokyo, Japan). Finally, the morphology and length of tracheal epithelial cilia were observed using an SEM. We determine the mean length of cilia observed in scanning electron microscopy images. Trachea rings from three rats of each experimental group were collected and prepared for scanning electron microscopy samples. A minimum of three images were captured for each sample of trachea ring sections. Subsequently, five fields, including at least five ciliated cells, were randomly selected from each image. From each of these ciliated cells, three cilia were randomly selected and their lengths were measured and quantified for the mean length of cilia in the SEM images (12,000× magnification). The distribution of cilia length was assessed by employing the frequency histogram distribution tool in GraphPad Prism.

Transmission Electron Microscopy (TEM)

The tracheas of three anesthetized rats from each group were dissected into small sections (1 × 1 × 1 mm) and subsequently fixed in a 2.5% glutaraldehyde solution with a pH of 7.4 for a duration of 6–8 h at 4°C. Subsequently, the specimens underwent a washing process and were then subjected to post-fixation in a 1% OsO_4 solution for a duration of 1 h at 4°C. These tissues were then subjected to dehydration using ethanol concentrations that varied incrementally, followed by embedding in araldite CY212. Semi-thin sections (1 μm) were subsequently sliced and subjected to staining with toluidine blue. Furthermore, ultra-thin sections (60–80 nm) were sliced and subjected to staining with uranyl acetate and alkaline lead citrate and analyzed using a Hitachi HT7700 electron microscope. A minimum of three images were captured for each sample of trachea ring sections. Subsequently, 10 cilia were randomly selected from each image to evaluate their ultrastructure. A total of 90 cilia were detected in each group. The ratio of abnormal cilia including cilia membrane blisters, dynein arm defects, and microtubules defects was quantified.

Analysis of Ciliary Orientation

Ciliary orientations were quantified as described previously.[28,29] At least 10 ciliary cross-sections were captured from each field at a magnification of 15,000×. On each image, a line was drawn at the center pair of each cross-section, and the angle of each line was measured (horizontal to the right = 0°; horizontal to the left = 180°). The mean SD of the ciliary

axis represents the overall measurement of ciliary disorientation in this subject. Each rat had five images selected, and three rats were selected from each group randomly.

Ultrastructure Analysis of Cilia

Three rats were selected at random from each group, and 3–5 images were randomly selected for each rat. The total number of cilia and the number of abnormal cilia, including ciliary membrane blister, dynein arm defects, microtubule defects, complex cilia, and megacilia, were counted by TEM, and the percentage of abnormal cilia was calculated.

Statistical Analysis

Data analysis was conducted using SPSS 26.0 (IBM; Armonk, NY, USA). The mean ± SD was used to express all data. Statistical differences between groups were assessed through a one-way analysis of variance (ANOVA). A significance level of $p < 0.05$ was deemed significant.

Results

LHQK Ameliorated Inflammatory Cell Infiltration and Airway Goblet Hyperplasia in Rats with AECOPD

To investigate the pharmaceutical effects of LHQK in a rat AECOPD model established by CS exposure and LPS intratracheal instillation (CS+LPS), morphological analysis by H&E staining (Figure 1A) and histochemistry staining for goblet cells (Muc5ac+) (Figure 1B) were performed. Notably, CS+LPS led to a noticeable infiltration of inflammatory cells and prominent morphological changes, such as alteration of composition and structure of airway epithelial cells and thickening of alveolar septa (Figure 1A). Furthermore, elevated Muc5ac+ cell number by histochemistry staining indicated goblet cell hyperplasia in AECOPD group ($p < 0.01$) (Figure 1B and C), confirming the successful establishment of AECOPD model in rats. Moreover, LHQK treatment exhibited a significant reduction in inflammatory cell infiltration (Figure 1A), a decrease in bronchial epithelial cell exfoliation (Figure 1A), and a prevention of the increase in the number of Muc5ac+ goblet cells ($P < 0.05$ or $p < 0.01$) (Figure 1B and C) induced by CS+LPS exposure. These findings provide evidence for the beneficial therapeutic effects of LHQK in rats with AECOPD.

LHQK Maintained the Ciliated Cell Proportion in Rats with AECOPD

Given that MCC plays an important role in airway mucus clearance and ciliated cells are a crucial component of the MCC system, we first conducted immunofluorescence staining (Figure 2A) and Western blot analysis (Figure 2B and C) using a ciliated cell-specific marker (anti-β-tubulin IV antibody) to investigate the alterations of ciliated cells. Compared with the control group, CS+LPS exposure significantly reduced the ciliated cell proportion in the lungs of the rats ($p < 0.01$). Additionally, LHQK and ELP treatment maintained β-tubulin IV positive ciliated cells ($p < 0.05$), indicating the potential role of LHQK in preventing ciliated cell loss in rats with AECOPD.

Ciliated cells are terminally differentiated cells[30] originating from upstream epithelial progenitor cells, such as basal cells and club cells upon injury stimulation.[31] Multiciliate Differentiation and DNA Synthesis Associated Cell Cycle Protein (MCIDAS) and forkhead box J1 (Foxj1) are two critical genes necessary for the generation of ciliated cells in respiratory epithelium.[32] Therefore, we evaluated the mRNA levels of *MCIDAS* (Figure 2D) and *Foxj1* (Figure 2E) using RT-qPCR. The results showed that the mRNA levels of MCIDAS ($p < 0.01$) and Foxj1 were significantly reduced ($p < 0.01$) in the CS+LPS group relative to the control group, indicating impaired ciliated cell differentiation in rat with AECOPD. Notably, the reduced mRNA levels of MCIDAS and Foxj1 were significantly attenuated upon LHQK and ELP treatment ($p < 0.05$ or $p < 0.01$). These results proved that LHQK maintains ciliated cell proportion probably by promoting ciliated cells differentiation. Of note, how LHQK modulates these differentiation processes deserves to be further investigated in the future.

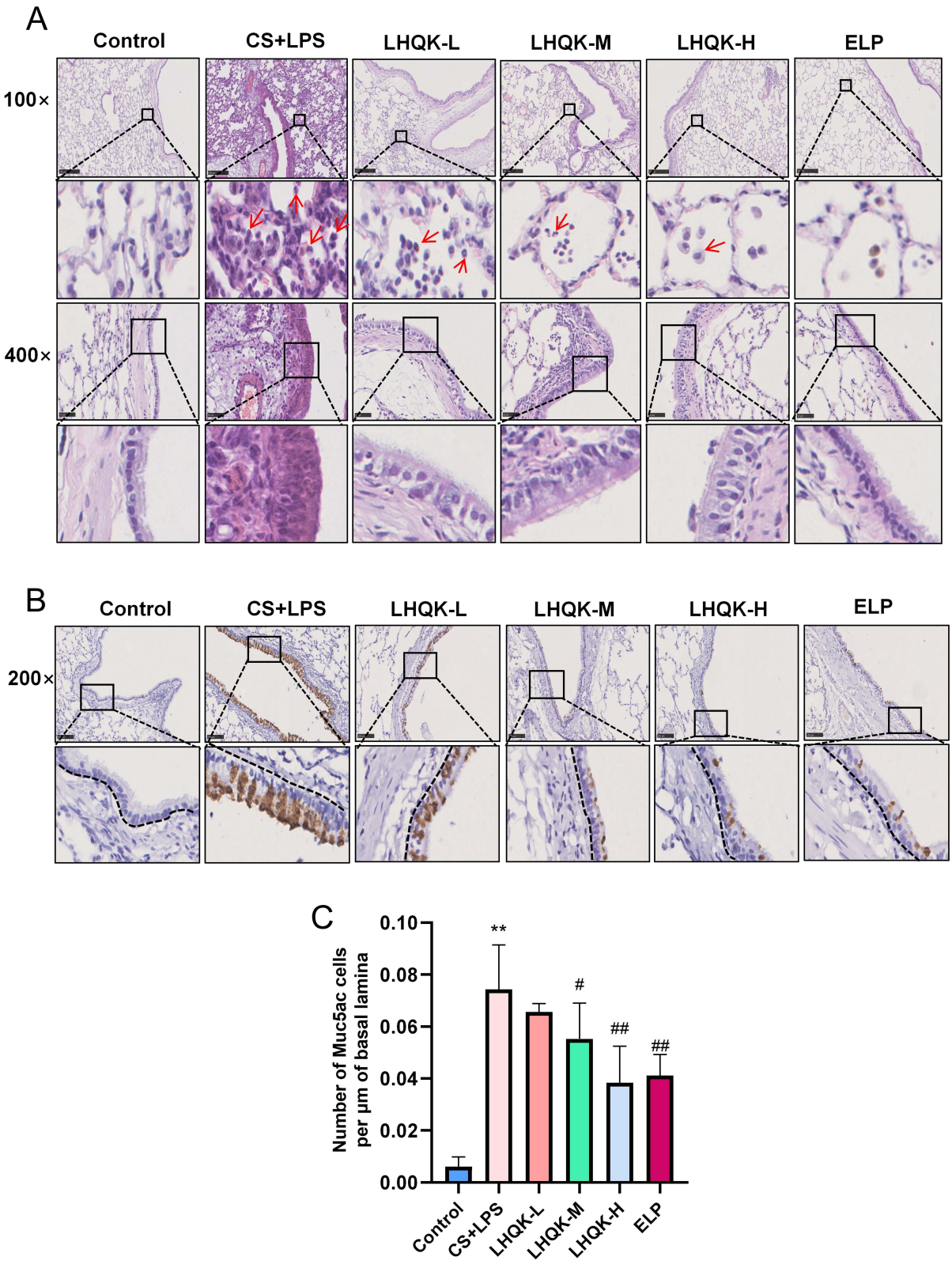

Figure 1 LHQK ameliorated the inflammatory cell infiltration and goblet hyperplasia in lung tissues of rats with AECOPD. (**A**) H&E staining of lung sections with multiple magnifications (100×,400×). Red arrows indicate immune cells. Scale bars are 250 μm (100×) and 50 μm (400×), respectively. (**B**) Immunohistochemistry staining of Muc5ac on sections from bronchial mucosa of rats (200×). The dashed lines represent the length of the basal lamina. Scale bars: 100 μm. (**C**) Number of cells per μm of basal lamina were shown as the mean ± SD (n = 5). $^{**}p < 0.01$ vs the control group; $^{\#}p < 0.05$, $^{\#\#}p < 0.01$ vs the CS+LPS group.

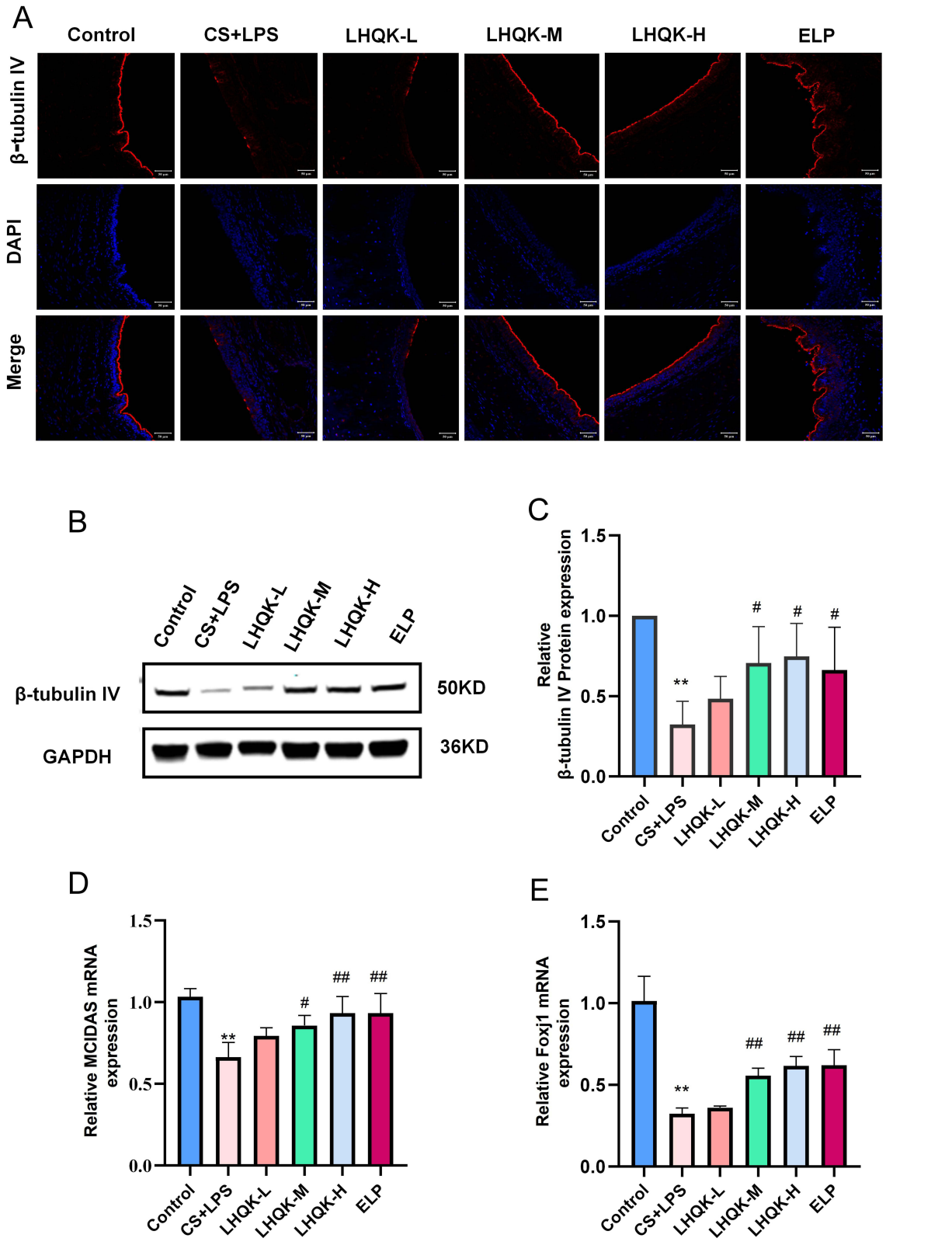

Figure 2 CS+LPS decreased the number of airway epithelial cilia, whereas LHQK increased the number of airway epithelial cilia. (**A**) Expression of cilia-associated protein β-tubulin IV was detected by immunofluorescence. Red light is β-tubulin IV (cilia-specific marker), and blue light is the nucleus (400×). Scale bars = 50 μm. (**B** and **C**) Expression of cilia-associated protein β-tubulin IV in the trachea was analyzed by Western blot analysis. n = 3. The data are shown as the mean ± SD. $^{**}p < 0.01$ vs. the control group; $^{\#}p < 0.05$ vs the CS+LPS group. (**D**) RT-qPCR analysis of the mRNA expression of the cilia-related gene MCIDAS; n = 3. The data are shown as the mean ± SD. $^{**}p < 0.01$ vs the control group; $^{\#}p < 0.05$ vs the CS+LPS group; $^{\#\#}p < 0.01$ vs the CS+LPS group. (**E**) RT-qPCR analysis of the mRNA expression of the cilia-related gene Foxj1; n = 3. The data are shown as the mean ± SD. $^{**}p < 0.01$ vs the control group; $^{\#\#}p < 0.01$ vs the CS+LPS group.

LHQK Ameliorated Cilia Loss and Shortening Triggered by CS+LPS Exposure in Rats with AECOPD

Cilia, which are specialized organelles located on the surface of ciliated cells, play a crucial role in MCC. Numerous studies have demonstrated the impact of cilia abnormalities, such as changes in ciliary density, length, CBF, ciliary-beat orientation, and ciliary ultrastructure, on MCC.[33] In line with this, H&E staining and SEM were employed to assess the ciliary length (μm). The results revealed a tendency of reduction in ciliary density in the CS+LPS group, whereas an increase was observed in the LHQK-M, LHQK-H, and ELP groups (Figure 3A). Additionally, SEM analysis provides a closer view of cilia from both transverse (Figure 3B) and longitudinal directions (Figure 3C). Ciliary length quantification results indicated that impaired ciliary length was ameliorated upon LHQK and ELP treatment

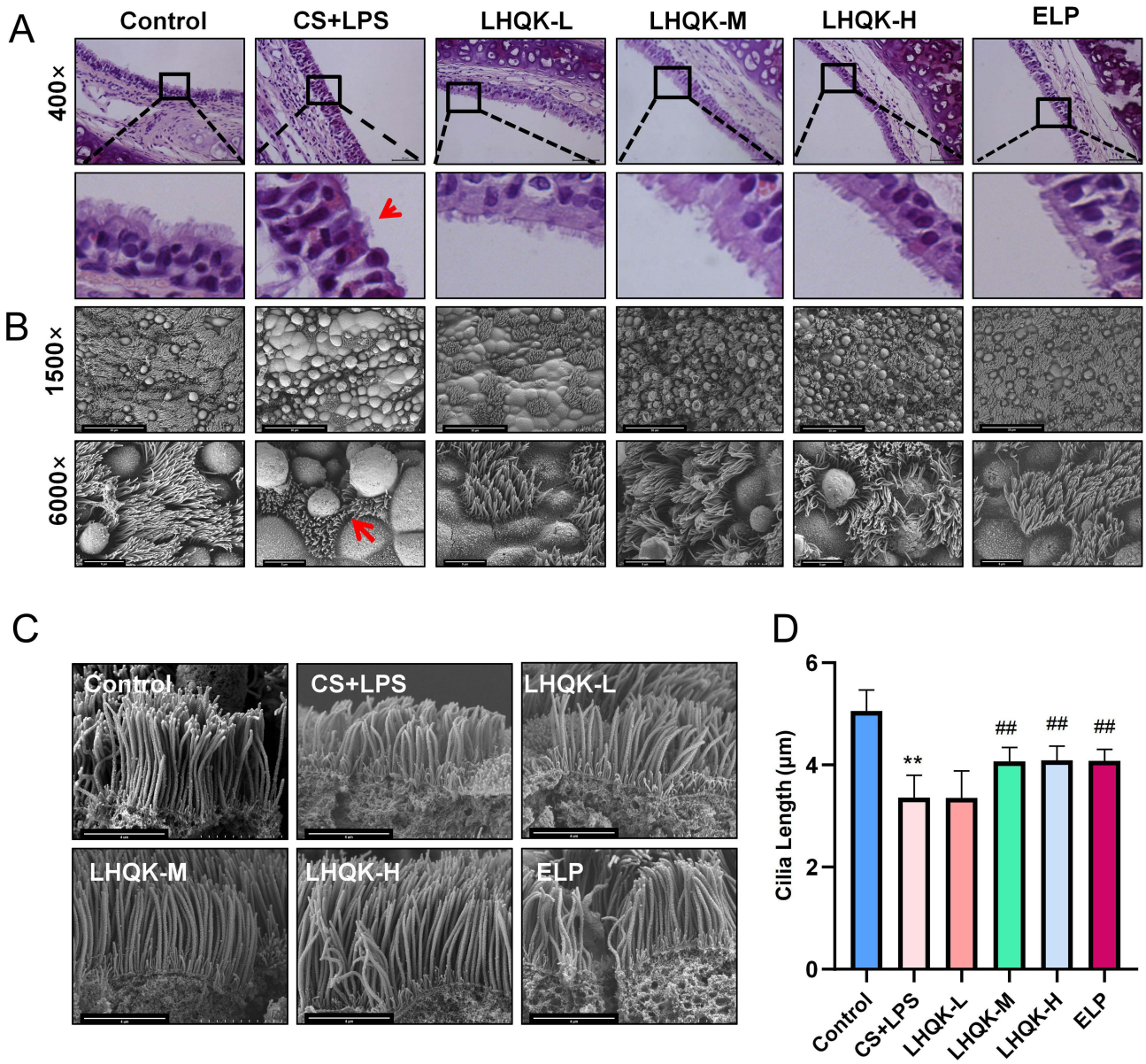

Figure 3 LHQK preserved the morphology of airway epithelial cilia in rats with AECOPD. (**A**) H&E staining of the trachea (400×). Scale bars: 50 μm. Red arrows indicate ciliated cells with shortened cilia. (**B**) Transverse section of trachea under SEM (1500×, 6000×). Red arrows indicate shortened cilia. Scale bars are 30 μm and 5 μm in (1500×) and in (6000×) images, respectively. (**C**) SEM longitudinal section (12,000×). Scale bars: 4 μm. (**D**) Ciliary length (μm). The data are shown as the mean ± SD. $^{**}p < 0.01$ vs the control group; $^{\#\#}p < 0.01$ vs the CS+LPS group.

(Figure 3C and D) ($p < 0.01$). Together, these results demonstrate the therapeutic capability of LHQK on maintaining ciliary density and length in rat AECOPD.

LHQK Preserved CBF in Rats with AECOPD

Next, to evaluate the CBF of bronchial cilia, both videos of ciliated cells on the tracheal rings and single isolated ciliated cells were captured using high-speed cameras (Supplementary videos 1, 2, 3, 4, 5 and 6) and analyzed with Image J in Figure 4. The ex vivo CBF analysis revealed that the CBF was significantly reduced after CS+LPS exposure ($p < 0.01$) but significantly improved in the LHQK-M, LHQK-H, and ELP groups ($p < 0.01$) (Figure 4A and B). Similarly, the in vitro CBF analysis also indicated a significantly impaired CBF of single ciliary cells isolated from the tracheas of rats in the CS+LPS group ($p < 0.01$), which was effectively ameliorated upon LHQK and ELP treatment ($p < 0.01$) (Figure 4C). These results indicate the therapeutic potential of LHQK in improving CBF in rats with AECOPD.

LHQK Reduced Ciliary Ultrastructural Damage in Rats with AECOPD

Given that ciliary structure integrity is an important factor influencing the proper beating function of cilia, the ultrastructure of cilia was evaluated by TEM. Ciliary defects such as a reduced number of cilia, an unequal diameter of the cilia, and uneven ciliary distribution were observed upon CS+LPS exposure (Figure 5A). Although morphological defects of cilia were observed in the LHQK-M and LHQK-H groups, the relatively quantified number was much lower than that in the CS+LPS group. Further quantification results indicated that the number of cilia with ciliary ultrastructure damages including the abnormal percentage of ciliary membrane blisters, the abnormal percentage of dynein arm defects, and the abnormal percentage of central or peripheral microtubule displacement were significantly higher in CS+LPS group than those in the control group ($p < 0.01$) (Figure 5B–D). Moreover, the relative cilia numbers with ciliary membrane blisters, dynein arm defects, or central or peripheral microtubule displacement were significantly reduced upon LHQK and ELP treatment ($p < 0.01$) (Figure 5B–D). These results reveal the protective effect of LHQK on ciliary ultrastructure.

LHQK Attenuated Random Ciliary Oscillations Caused by AECOPD

Finally, ciliary orientations were quantified as described previously[28,29] by measuring the ciliary deviation in electron micrographs (Figure 6A–C). The results show that ciliary direction is disordered in the CS+LPS group ($p < 0.01$). However, the ciliary direction of specimens in the LHQK- L($P < 0.05$), LHQK-M ($p < 0.01$), LHQK-H ($p < 0.01$), and ELP groups ($p < 0.01$) was relatively constant, indicating the therapeutic property of LHQK on regulating ciliary orientation.

Discussion

CS stands as the paramount risk factor for COPD,[34,35] whereas LPS instillation is useful in constructing a short-term animal model of COPD with relative features of human disease.[36,37] When CS and LPS are administered concomitantly, they can induce AECOPD,[38] which typically manifests as mucus hypersecretion and impairment of MCC.[39] In this study, we show that LHQK attenuates the disturbed airway epithelial proportion including goblet hyperplasia, and ciliated cell loss induced by CS+LPS exposure. In addition, we proved that LHQK could increase ciliary density and length, ameliorate ciliary ultrastructural abnormalities and disturbed ciliary orientation, and ameliorate abnormal CBF caused by CS+LPS exposure.

MCC is a crucial defense mechanism that relies on the cooperation between goblet and ciliated cells in the lung.[40] In healthy lungs, goblet cells secret mucus that covers the surface of the respiratory epithelium and traps harmful particles and pathogens. Ciliated cells form hundreds of motile cilia that beat in metachronal waves to expel the mucus that traps inhaled particles and pathogens out of the airways. A variety of respiratory diseases are characterized by excessive mucus production, ciliated cell loss, and impaired ciliary structure and beat function, leading to dysfunctional MCC.[41,42] To evaluate the therapeutic effects of LHQK on airway ciliated cells in rat with AECOPD, we assessed airway cell populations of goblet cells and ciliated cells using immunohistochemical and immunofluorescence staining. The results showed that LHQK attenuated goblet hyperplasia and ciliated cell loss induced by CS+LPS exposure. Given that

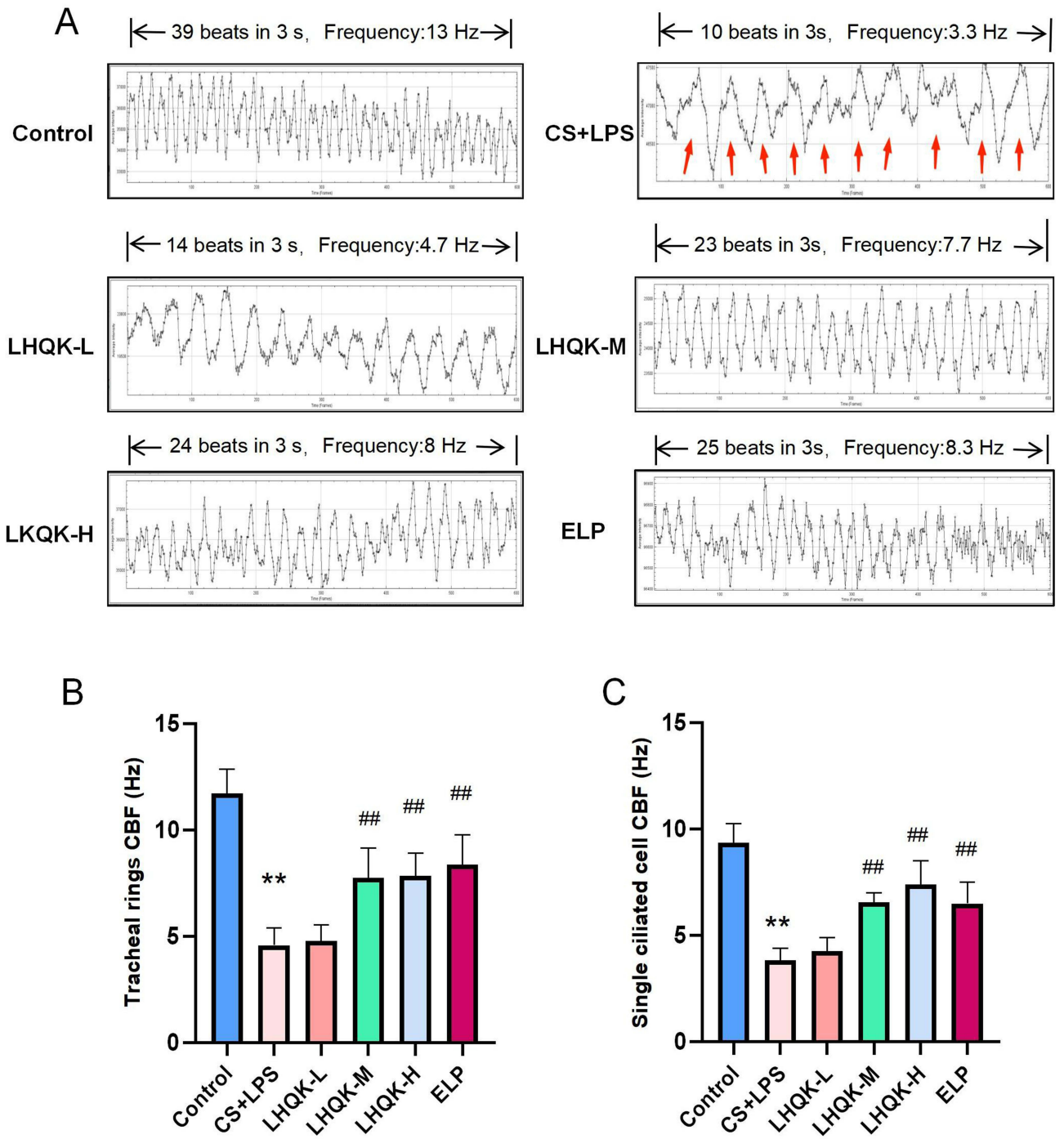

Figure 4 LHQK reversed the reduced CBF of ciliated cells in rats with AECOPD. (**A**) Image J software was used to analyze the tracheal ring CBF. The red arrow indicates that the cilia wiggled once. (**B**) Trachea ring CBF (n = 3). $^{**}p < 0.01$ vs the control group; $^{\#\#}p < 0.01$ vs the CS+LPS group. (**C**) CBF of ciliary cells in vitro (n = 3). $^{**}p < 0.01$ vs the control group; $^{\#\#}p < 0.01$ vs. the CS+LPS group.

impaired ciliated cell differentiation may contribute to the loss of ciliated cells, we evaluated the mRNA levels of two critical genes (MCIDAS and Foxj1) critical for ciliated cell differentiation. We found that the transcription levels of these two genes were significantly rescued following LHQK treatment relative to CS+LPS exposure, indicating that LHQK suppresses mucus hypersecretion and maintains airway epithelial homeostasis by promoting ciliated cell differentiation.

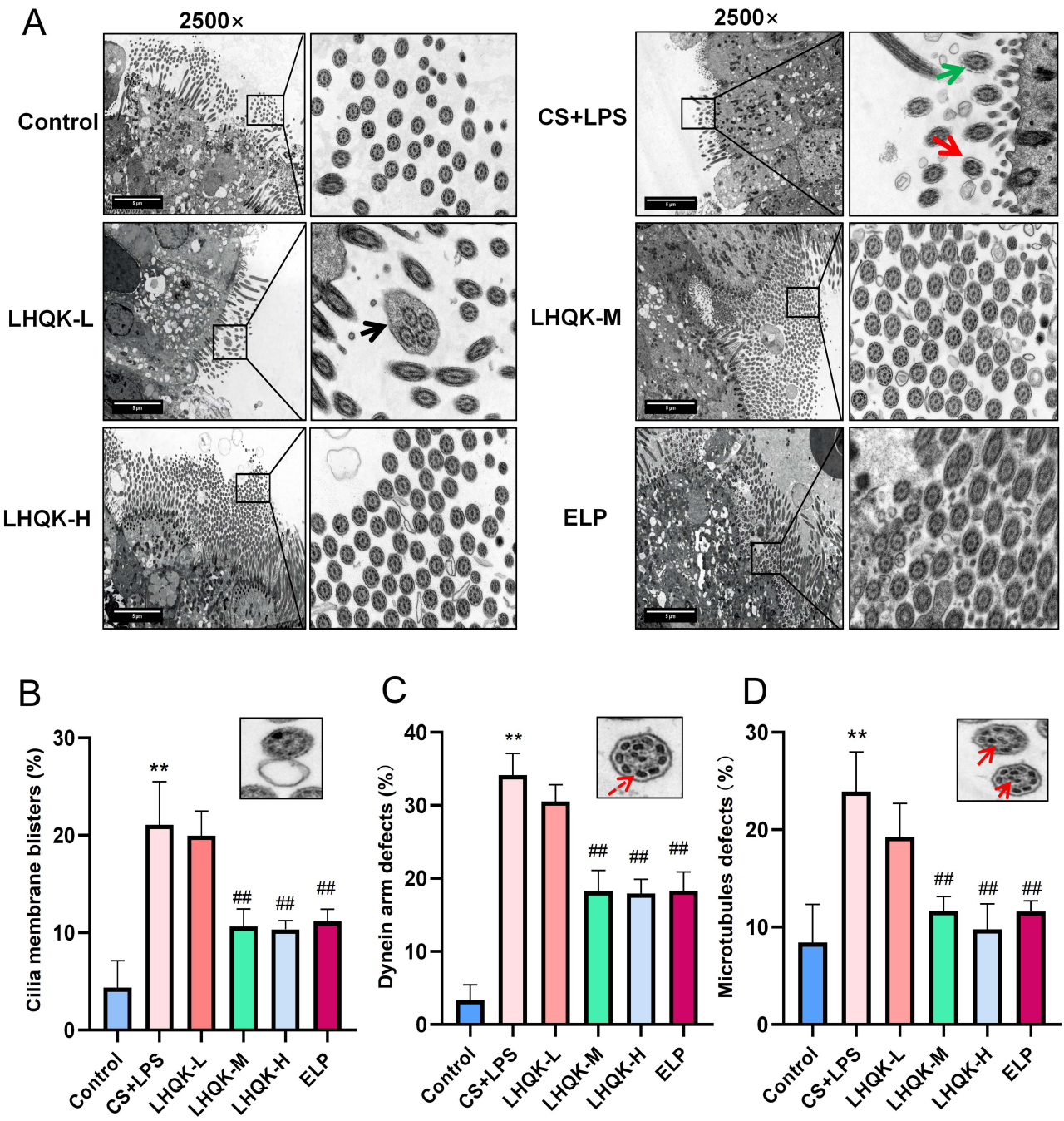

Figure 5 LHQK reduced ciliary ultrastructural damage caused by CS+LPS exposure. (**A**) TEM images (2500×) and enlarged images show the ultrastructure of cilia on the surface of ciliated cells. The green arrows indicate broken and disintegrating ciliary membranes. The black arrows show compound cilia. The red arrow shows the ciliary membrane blister. Scale bars: 5 μm. (**B**) Abnormal percentage of ciliary membrane blisters (n = 3). $^{**}p < 0.01$ vs the control group; $^{\#\#}p < 0.01$ vs the CS+LPS group; (**C**) Abnormal rate of dynein arm defects (n = 3). $^{**}p < 0.01$ vs the control group; $^{\#\#}p < 0.01$ vs the CS+LPS group. The red dotted arrow is the defects of the dynein arm. (**D**) Abnormal rate of microtubule defects (n = 3). $^{**}p < 0.01$ vs the control group; $^{\#\#}p < 0.01$ vs the CS+LPS group. Solid red arrows indicate microtubule displacement. Representative images of ciliary damage were shown on the right corner of bar results in (**B**–**D**).

However, considering that ciliated cells could originate from multiple airway epithelial progenitor cells including basal cells and club cells, the exact molecular mechanisms regulating ciliated cell differentiation in AECOPD deserve to be further investigated.

Cilia located on the apical surface of ciliated cells exhibit coordinated beating patterns, facilitating the transportation of mucus towards the pharynx.[31] Any structural or functional impairment of cilia can negatively impact MCC,[43] leading

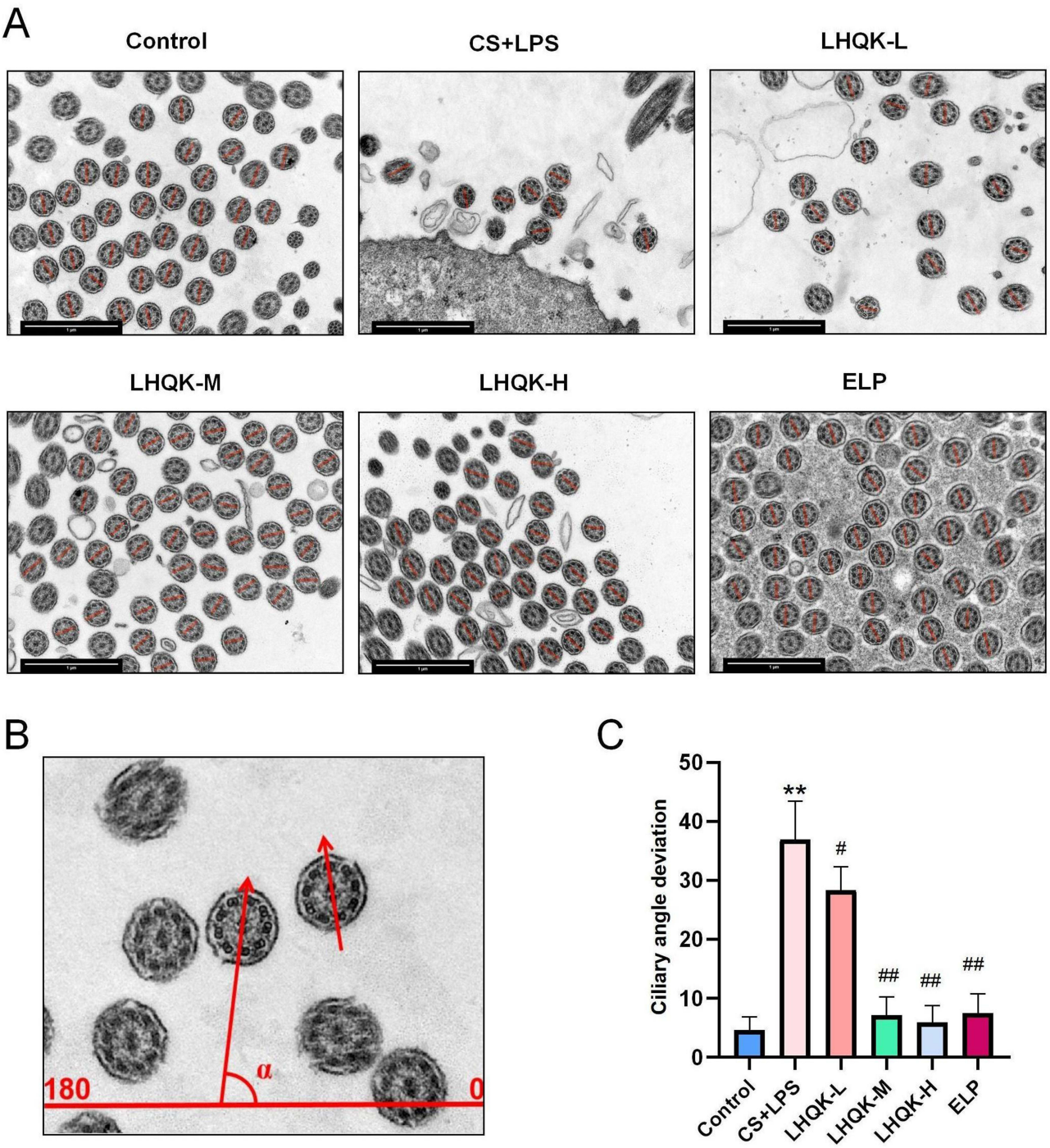

Figure 6 LHQK preserved random ciliary oscillations triggered by CS+LPS exposure. (**A**) TEM images (15,000×) are labeled with red lines crossing the central microtubules, which is called the axis of cilia. Scale bars: 1 μm. (**B**) Schematic diagram of the ciliary axis angle measurement. (**C**) Ciliary angle deviation. $^{**}p < 0.01$ vs the control group; $^{\#}P < 0.05$, $^{\#\#}p < 0.01$ vs the CS+LPS group.

to a higher risk of respiratory infections.[14] To assess the effect of LHQK on MCC, we evaluated the ciliary density and length, which are two critical parameters for MCC.[18] We found that LHQK increased both ciliary density and length, which were decreased by CS+LPS exposure. It has been proven that ciliary autophagy contributes to cilia shortening.[39,44] Thus, it would be worth investigating whether LHQK regulates ciliary length via the autophagy pathway.

Moreover, proper CBF is another critical determinant of MCC because it helps to promote sputum expulsion.[45] Impaired CBF can lead to increased mucus secretion, which is characteristic of COPD.[46] Proper CBF relies on the intact ultrastructure and orientation of the cilia.[13,47–49] Previous studies have demonstrated that smokers and ex-smokers have a higher degree of ciliary ultrastructural abnormalities than non-smokers.[48] Additionally, random ciliary orientation, an important factor affecting the CBF, has also been reported as a possible cause of COPD.[15,28] In this study, we evaluated and quantified the CBF, ultrastructure, and orientation of cilia. Our findings reveal that CS+LPS exposure enhanced the ciliary ultrastructural abnormalities, disturbed the ciliary orientation, and led to an abnormal CBF. However, treatment with LHQK significantly ameliorated these effects, indicating its potential role in improving MCC by maintaining proper CBF via the regulation of the ciliary ultrastructure and orientation.

Finally, the difficulty of studying the pharmacological mechanisms of TCM formulas is a long-standing issue. Generally, the pharmacological mechanism of a compound traditional Chinese medicine (cTCM) is usually complex and involves multiple components, targets, pathways, and interactions. Despite the limitations of this study in elucidating precise molecular mechanisms, this first study providing evidence for the multiple therapeutic effects of LHQK on MCC in AECOPD. Further studies are needed to identify the specific active components of LHQK that modulate ciliated cell and cilia-related MCC molecular mechanisms in AECOPD.

Conclusion

Our results indicate that treatment with LHQK is beneficial to rats with AECOPD. Furthermore, we have successfully recapitulated the effects of LHQK treatment on the enhancement of MCC. LHQK enhances MCC by preventing goblet cell hyperplasia, preserving ciliated cell population, and safeguarding the structural and functional integrity of cilia on the surface of ciliated cells. Additionally, LHQK exerts its protective effects on cilia by increasing ciliary density and length, as well as improving the ciliary ultrastructure, orientation, and CBF. Nevertheless, further investigations are needed to elucidate the precise underlying molecular mechanisms involved in these processes.

Author Contributions

All authors made a significant contribution to the work reported, whether in the conception, study design, execution, acquisition of data, analysis and interpretation, or in all of these areas. All authors took part in drafting, revising, or critically reviewing the article, gave final approval for the version to be published, have agreed on the journal to which the article has been submitted and agreed to be accountable for all aspects of the work.

Funding

This work was funded by the Innovation Team and Talents Cultivation Program of National Administration of Traditional Chinese Medicine [No. ZYYCXTD-D-202206], Key Project of National Natural Science Foundation of China [NO.82130123], Natural Science Foundation of Hebei Province [NO. H2023106039], Scientific Research Project of Hebei Provincial Administration of Traditional Chinese Medicine [2024401].

Disclosure

The authors declare that they have no known competing financial interests or personal relationships that could have appeared to influence the work reported in this paper.

References

1. Singh D, Agusti A, Anzueto A, et al. Global strategy for the diagnosis, management, and prevention of chronic obstructive lung disease: the GOLD science committee report 2019. *Eur Respir J*. 2019;53(5):1900164. doi:10.1183/13993003.00164-2019
2. Venkatesan P. GOLD COPD report: 2023 update. *Lancet Respir Med*. 2023;11(1):18. doi:10.1016/s2213-2600(22)00494-5
3. MacLeod M, Papi A, Contoli M, et al. Chronic obstructive pulmonary disease exacerbation fundamentals: diagnosis, treatment, prevention and disease impact. *Respirology*. 2021;26(6):532–551. doi:10.1111/resp.14041
4. Ma Y, Huang K, Liang C, et al. Real-world antibiotic use in treating acute exacerbations of chronic obstructive pulmonary disease (AECOPD) in China: evidence from the ACURE study. *Front Pharmacol*. 2021;12:649884. doi:10.3389/fphar.2021.649884

5. Feng F, Du J, Meng Y, Guo F, Feng C. Louqin Zhisou Decoction Inhibits Mucus Hypersecretion For Acute Exacerbation Of Chronic Obstructive Pulmonary Disease Rats By Suppressing EGFR-PI3K-AKT signaling pathway and restoring Th17/Treg balance. *Evid Based Complement Alternat Med*. 2019;2019:6471815. doi:10.1155/2019/6471815
6. Ramos FL, Krahnke JS, Kim V. Clinical issues of mucus accumulation in COPD. *Int J Chron Obstruct Pulmon Dis*. 2014;9:139–150. doi:10.2147/copd.S38938
7. Sapey E, Stockley RA. COPD exacerbations. 2: aetiology. *Thorax*. 2006;61(3):250–258. doi:10.1136/thx.2005.041822
8. Hogg JC, Chu FS, Tan WC, et al. Survival after lung volume reduction in chronic obstructive pulmonary disease: insights from small airway pathology. *Am J Respir Crit Care Med*. 2007;176(5):454–459. doi:10.1164/rccm.200612-1772OC
9. Houtmeyers E, Gosselink R, Gayan-Ramirez G, Decramer M. Regulation of mucociliary clearance in health and disease. *Eur Respir J*. 1999;13(5):1177–1188. doi:10.1034/j.1399-3003.1999.13e39.x
10. Bustamante-Marin XM, Ostrowski LE. Cilia and mucociliary clearance. *Cold Spring Harb Perspect Biol*. 2017;9(4):a028241. doi:10.1101/cshperspect.a028241
11. Cao Y, Chen M, Dong D, Xie S, Liu M. Environmental pollutants damage airway epithelial cell cilia: implications for the prevention of obstructive lung diseases. *Thorac Cancer*. 2020;11(3):505–510. doi:10.1111/1759-7714.13323
12. Kuek LE, Lee RJ. First contact: the role of respiratory cilia in host-pathogen interactions in the airways. *Am J Physiol Lung Cell Mol Physiol*. 2020;319(4):L603–L619. doi:10.1152/ajplung.00283.2020
13. Yaghi A, Dolovich MB. Airway epithelial cell cilia and obstructive lung disease. *Cells*. 2016;5(4):40. doi:10.3390/cells5040040
14. Love ME, Proud D. Respiratory viral and bacterial exacerbations of COPD-the role of the airway epithelium. *Cells*. 2022;11(9):1416. doi:10.3390/cells11091416
15. Rutland J, de Iongh RU. Random ciliary orientation. A cause of respiratory tract disease. *N Engl J Med*. 1990;323(24):1681–1684. doi:10.1056/nejm199012133232406
16. Ballenger JJ. Experimental effect of cigarette smoke on human respiratory cilia. *N Engl J Med*. 1960;263(17):832–835. doi:10.1056/nejm196010272631704
17. Frasca JM, Auerbach O, Carter HW, Parks VR. Morphologic alterations induced by short-term cigarette smoking. *Am J Pathol*. 1983;111(1):11–20.
18. Leopold PL, O'Mahony MJ, Lian XJ, Tilley AE, Harvey BG, Crystal RG. Smoking is associated with shortened airway cilia. *PLoS One*. 2009;4(12):e8157. doi:10.1371/journal.pone.0008157
19. Haswell LE, Hewitt K, Thorne D, Richter A, Gaça MD. Cigarette smoke total particulate matter increases mucous secreting cell numbers in vitro: a potential model of goblet cell hyperplasia. *Toxicol In Vitro*. 2010;24(3):981–987. doi:10.1016/j.tiv.2009.12.019
20. Hsieh CF, Lo CW, Liu CH, et al. Mechanism by which ma-xing-shi-gan-tang inhibits the entry of influenza virus. *J Ethnopharmacol*. 2012;143(1):57–67. doi:10.1016/j.jep.2012.05.061
21. Zhen G, Jing J, Fengsen L. Traditional Chinese medicine classic herbal formula Xiaoqinglong decoction for acute exacerbation of chronic obstructive pulmonary disease: a systematic review protocol. *Medicine*. 2018;97(52):e13761. doi:10.1097/md.0000000000013761
22. Xiao S, Liu L, Sun Z, et al. Network pharmacology and experimental validation to explore the mechanism of Qing-Jin-Hua-Tan-decoction against acute lung injury. *Front Pharmacol*. 2022;13:891889. doi:10.3389/fphar.2022.891889
23. Wang M, Li W, Cui W, et al. The therapeutic promises of Lianhuaqingke in the mice model of coronavirus pneumonia (HCoV-229E and SARS-CoV-2). *Chin Med*. 2021;16(1):104. doi:10.1186/s13020-021-00513-3
24. Zhang L, Wu L, Xu X, et al. Efficacy and safety of lianhua qingke tablets in the treatment of mild and common-type COVID-19: a randomized, controlled, multicenter clinical study. *Evid Based Complement Alternat Med*. 2022;2022:8733598. doi:10.1155/2022/8733598
25. Gu C, Wang H, Zhu H, Wei G. Pharmacodynamics of Lianhua Jizhi tablets in the treatment of acute bronchitis. *Asia-Pacific J Tradit Chin Med*. 2015;11(09):9–11.
26. Ji C, Wei C, Li M, et al. Bazi Bushen capsule attenuates cognitive deficits by inhibiting microglia activation and cellular senescence. *Pharm Biol*. 2022;60(1):2025–2039. doi:10.1080/13880209.2022.2131839
27. Wyatt TA, Gentry-Nielsen MJ, Pavlik JA, Sisson JH. Desensitization of PKA-stimulated ciliary beat frequency in an ethanol-fed rat model of cigarette smoke exposure. *Alcohol Clin Exp Res*. 2004;28(7):998–1004. doi:10.1097/01.alc.0000130805.75641.f4
28. Rautiainen ME. Orientation of human respiratory cilia. *Eur Respir J*. 1988;1(3):257–261. doi:10.1183/09031936.93.01030257
29. de Iongh R, Ing A, Rutland J. Mucociliary function, ciliary ultrastructure, and ciliary orientation in young's syndrome. *Thorax*. 1992;47(3):184–187. doi:10.1136/thx.47.3.184
30. Rogers DF, Barnes PJ. Treatment of airway mucus hypersecretion. *Ann Med*. 2006;38(2):184–187. doi:10.1136/thx.47.3.184
31. Tilley AE, Walters MS, Shaykhiev R, Crystal RG. Cilia dysfunction in lung disease. *Annu Rev Physiol*. 2015;77(1):379–406. doi:10.1146/annurev-physiol-021014-071931
32. Boon M, Wallmeier J, Ma L, et al. MCIDAS mutations result in a mucociliary clearance disorder with reduced generation of multiple motile cilia. *Nat Commun*. 2014;5(1):4418. doi:10.1038/ncomms5418
33. Hadi SM, Sasan S, Omid A. Three-dimensional simulation of mucociliary clearance under the ciliary abnormalities. *J Nonnewton Fluid Mech*. 2023;316:105029.
34. Mannino DM, Buist AS. Global burden of COPD: risk factors, prevalence, and future trends. *Lancet*. 2007;370(9589):765–773. doi:10.1016/s0140-6736(07)61380-4
35. Li Y, Li SY, Li JS, et al. A rat model for stable chronic obstructive pulmonary disease induced by cigarette smoke inhalation and repetitive bacterial infection. *Biol Pharm Bull*. 2012;35(10):1752–1760. doi:10.1248/bpb.b12-00407
36. Wright JL, Churg A. Animal models of COPD: barriers, successes, and challenges. *Pulm Pharmacol Ther*. 2008;21(5):696–698. doi:10.1016/j.pupt.2008.01.007
37. Ghorani V, Boskabady MH, Khazdair MR, Kianmeher M. Experimental animal models for COPD: a methodological review. *Tob Induc Dis*. 2017;15(1):25. doi:10.1186/s12971-017-0130-2
38. Wright JL, Cosio M, Churg A. Animal models of chronic obstructive pulmonary disease. *Am J Physiol Lung Cell Mol Physiol*. 2008;295(1):L1–L15. doi:10.1152/ajplung.90200.2008
39. Cloonan SM, Lam HC, Ryter SW, Choi AM. "Ciliophagy": the consumption of cilia components by autophagy. *Autophagy*. 2014;10(3):532–534. doi:10.4161/auto.27641

40. Gohy S, Carlier FM, Fregimilicka C, et al. Altered generation of ciliated cells in chronic obstructive pulmonary disease. *Sci Rep*. 2019;9(1):17963. doi:10.1038/s41598-019-54292-x
41. Roy MG, Livraghi-Butrico A, Fletcher AA, et al. Muc5b is required for airway defence. *Nature*. 2014;505(7483):412–416. doi:10.1038/nature12807
42. Walentek P. Signaling control of mucociliary epithelia: stem cells, cell fates, and the plasticity of cell identity in development and disease. *Cells Tissues Organs*. 2022;211(6):736–753. doi:10.1159/000514579
43. Li YY, Liu J, Li CW, et al. Myrtol standardized affects mucociliary clearance. *Int Forum Allergy Rhinol*. 2017;7(3):304–311. doi:10.1002/alr.21878
44. Lam HC, Cloonan SM, Bhashyam AR, et al. Histone deacetylase 6-mediated selective autophagy regulates COPD-associated cilia dysfunction. *J Clin Invest*. 2013;123(12):5212–5230. doi:10.1172/jci69636
45. Clapp PW, Lavrich KS, van Heusden CA, et al. Cinnamaldehyde in flavored e-cigarette liquids temporarily suppresses bronchial epithelial cell ciliary motility by dysregulation of mitochondrial function. *Am J Physiol Lung Cell Mol Physiol*. 2019;316(3):L470–L486. doi:10.1152/ajplung.00304.2018
46. Yaghi A, Zaman A, Cox G, Dolovich MB. Ciliary beating is depressed in nasal cilia from chronic obstructive pulmonary disease subjects. *Respir Med*. 2012;106(8):1139–1147. doi:10.1016/j.rmed.2012.04.001
47. Joki S, Toskala E, Saano V, Nuutinen J. Correlation between ciliary beat frequency and the structure of ciliated epithelia in pathologic human nasal mucosa. *Laryngoscope*. 1998;108(3):426–430. doi:10.1097/00005537-199803000-00021
48. Wang WJ, Yang SF, Gao ZR, Luo ZR, Liu YL, Gao XL. MIP-T3 expression associated with defects of ciliogenesis in airway of COPD patients. *Can Respir J*. 2020;2020:1350872. doi:10.1155/2020/1350872
49. Cutz E, Levison H, Cooper DM. Ultrastructure of airways in children with asthma. *Histopathology*. 2002;41(3a):22–36.

International Journal of Chronic Obstructive Pulmonary Disease Dovepress

Publish your work in this journal

The International Journal of COPD is an international, peer-reviewed journal of therapeutics and pharmacology focusing on concise rapid reporting of clinical studies and reviews in COPD. Special focus is given to the pathophysiological processes underlying the disease, intervention programs, patient focused education, and self management protocols. This journal is indexed on PubMed Central, MedLine and CAS. The manuscript management system is completely online and includes a very quick and fair peer-review system, which is all easy to use. Visit http://www.dovepress.com/testimonials.php to read real quotes from published authors.

Submit your manuscript here: https://www.dovepress.com/international-journal-of-chronic-obstructive-pulmonary-disease-journal